

# Eutectic Mesophase Transitions and Induced Crystalline Phase in Mixtures of Hexagonal Columnar Liquid Crystal and Mesogenic Diacrylate

Tsang-Min Huang,<sup>†</sup> Raisa V. Talroze,<sup>‡</sup> and Thein Kyu\*,<sup>†</sup>

Department of Polymer Engineering, University of Akron, Akron, Ohio 44325, and Topchiev Institute of Petrochemical Synthesis, Russian Academy of Sciences, Moscow, Russia

Received: May 26, 2010; Revised Manuscript Received: August 18, 2010

Eutectic behavior and the induced crystalline phase in mixtures of hexagonal columnar liquid crystal, 2, 3, 6, 7, 10, 11-hexakis-(pentyloxy) triphenylene (HPTP)/reactive mesogenic diacrylate monomer, 4-(3-acryloyloxypropoxyloxy)-benzoic acid 2-methyl-1, 4-phenylene ester (RM257) have been investigated both experimentally and theoretically. To determine the theoretical phase boundaries, we combined the free energy of Flory–Huggins free energy for liquid–liquid demixing, Maier–Saupe free energy of nematic ordering, and Chandrasekhar–Clark free energy of hexagonal ordering. The calculated phase diagram of the HPTP/RM257 blend is essentially of a eutectic type that consists of isotropic (I), nematic (N), and hexagonal columnar ( $Col_h$ ) regions, and nematic + isotropic (N+I), hexagonal columnar + isotropic ( $Col_h$ +I), and hexagonal columnar + nematic ( $Col_h$ +N) coexistence regions, bound by the liquidus and solidus lines. Of particular interest is the formation of an induced crystalline phase ( $Cr_{in}$ ) in the intermediate compositions of the HPTP/RM257 mixtures, exhibiting  $Cr_2$  (RM257) +  $Cr_{in}$  in the RM257-rich and  $Cr_{in}$  +  $Cr_I$  (HPTP) in the HPTP-rich regions.

## Introduction

Columnar liquid crystals, having considerable overlapped orbitals of adjacent cores, commonly exhibit higher conductivity in the columnar direction relative to the transverse direction, which is known as quasi-one-dimensional conductivity.<sup>1,2</sup> The transports of charges and excitons are faster in the columnar liquid crystals than in the conventional conjugated polymers.<sup>3</sup> Consequently, these columnar liquid crystals (CLC) have found potential applications in various electro-optical devices such as organic light-emitting diodes (OLED), organic field effect transistors (OFET), and organic photovoltaics (OPV).<sup>4–8</sup> Evidently, the performance of these devices can be optimized by controlling the orientation of the CLC columns along the thickness direction, which can be realized by employing a thermal gradient, mechanical, electrical, or magnetic fields, etc.<sup>9,10</sup>

In an effort to align the CLC cylinders in the film normal direction, we have used the wave interference patterning approach in photolithography. The feasibility of fabricating such aligned arrays of nematic LC cylinders has already been demonstrated by numerical computation based on the principles of photolithographic photopolymerization-induced phase separation in comparison with the experimental results of polyethylene oxide/triacrylate blends.<sup>11,12</sup> Prior to performing photolithographic patterning of mixtures of columnar liquid crystals and photoreactive monomers, it is of utmost importance to better understand the phase diagram of the starting mixtures, which is the focus of the present work.

In this article, the columnar liquid crystal, viz., hexakis(pentyloxy)triphenylene (HPTP), was chosen because of its capability for homeotropic alignment. The reactive mesogenic diacrylate monomer (RM257) was selected as its counterpart because photopolymerized RM257 has superior thermal stability and low shrinkage as compared to conventional thermosets; therefore, it should provide excellent long-term stability of photonic

devices. First, the phase diagram of the HPTP/RM257 mixture was determined by means of differential scanning calorimetry (DSC), polarized optical microscopy (POM), and wide-angle X-ray diffraction (WAXD). Second, a theoretical phase diagram was constructed in the framework of the combined free energy of Flory–Huggins theory for liquid–liquid demixing, Maier–Saupe theory for nematic ordering, and Chandrasekhar–Clark theory for hexagonal columnar ordering. In descending order of temperature, the observed phase diagram shows isotropic (I), nematic (N), hexagonal columnar ( $Col_h$ ) regions, and nematic + isotropic (N+I), hexagonal columnar + isotropic ( $Col_h$ +I), and hexagonal columnar + nematic ( $Col_h$ +N) coexistence regions. Moreover, an induced crystalline phase ( $Cr_{in}$ ) develops in intermediate concentrations surrounded by the  $Cr_2$  (RM257) +  $Cr_{in}$  and  $Cr_{in}$  +  $Cr_I$  (HPTP) gaps. The complex phase behavior of these HPTP/RM257 mixtures is discussed with emphasis on the eutectic behavior of the mesophases and the induced crystalline phase.

## Experimental Section

**Materials.** The reactive nematic mesogen, 4-(3-acryloyloxypropoxyloxy)benzoic acid 2-methyl-1,4-phenylene ester (RM257), was purchased from Merck and used as received. RM257 exhibits a crystal–nematic transition ( $T_{Cr-N}$ ) at 65 °C and a nematic–isotropic transition ( $T_{N-I}$ ) at 127 °C. The columnar liquid crystal, viz., 2,3,6,7,10,11-hexakis(pentyloxy)triphenylene (HPTP), was synthesized in the laboratory of Dr. R. V. Talroze following the synthesis protocol of Boden and co-workers.<sup>13</sup> The as-synthesized HPTP shows a crystal–hexagonal columnar phase transition ( $T_{Cr-Colh}$ ) at 66 °C and a columnar–isotropic transition ( $T_{Colh-I}$ ) at 121 °C.

**Methods.** Various mixtures of HPTP/RM257 were dissolved in a common solvent, tetrahydrofuran (THF), by mechanically stirring until the solution became homogeneous. The blend film was solution-cast on glass substrates at ambient temperature and dried under vacuum at room temperature for 24 h to remove any residual solvent. The phase transition temperature of the

\* To whom correspondence should be addressed. E-mail: tkyu@uakron.edu.

<sup>†</sup> University of Akron.

<sup>‡</sup> Russian Academy of Sciences.

mixtures was determined by using differential scanning calorimeter (DSC, Model Q1000, TA Instruments). Temperature and enthalpy calibration were performed using an indium standard. The recommended amount (5–10 mg) of the sample was sealed in aluminum hermetic pans, and the DSC scans were acquired in the temperature range between 0 and 140 °C at a scan rate of 2 °C/min.

In the polarized optical microscopy (POM) experiments, an optical microscope (BX60, Olympus) equipped with a 35 mm camera (EOS 400D, Canon) and a hot stage (TMS93, Linkam) was utilized. The heating and cooling rates were 1 °C/min unless indicated otherwise.

Wide-angle X-ray diffraction (WAXD) experiments were carried out in the reflection mode using a rotating anode generator (Rigaku, 12 kW) and a diffractometer (Geigerflex, D/max-RB with a radius of 185 nm). The X-ray source was Cu K $\alpha$  with a wavelength of 0.154 nm. The diffraction peak positions and widths were calibrated with a known silicon crystal at a high angle region ( $2\theta \geq 15^\circ$ ) and silver behenate in a low angle region ( $2\theta \leq 15^\circ$ ). A sample hot stage was attached to the diffractometer for in situ investigation of the mesophase transitions during cooling and heating cycles.  $2\theta$ -WAXD (Bragg's angle) scans were acquired in the range from  $1.5^\circ$  to  $35^\circ$  at a scanning rate of 2°/min. The X-ray intensities at  $2\theta = 8$  or higher were magnified 10 fold to enhance the diffraction peaks.

### Theoretical Scheme

The total free energy of the hexagonal columnar LC/nematic mesogen mixture is expressed in terms of a combination of Flory–Huggins (FH) free energy density of liquid–liquid demixing and the anisotropic free energy density of liquid crystalline ordering,  $f^{\text{total}} = f^{\text{mixing}} + f^{\text{aniso}}$ . The FH free energy density of liquid–liquid demixing,  $f^{\text{mixing}}$ , is described as:<sup>14,15</sup>

$$f^{\text{mixing}} = \phi_1 \ln \phi_1/r_1 + \phi_2 \ln \phi_2/r_2 + \chi \phi_1 \phi_2 \quad (1)$$

where  $\phi_1$  and  $\phi_2$  represent the volume fractions of hexagonal columnar and nematic LCs, respectively.  $r_1$  and  $r_2$  are the numbers of statistical chain segments of the corresponding constituents.  $\chi$  is the Flory–Huggins interaction parameter, which is defined as  $\chi = A + B/T$  where  $A$  and  $B$  are constants related to entropic and enthalpic contributions to the free energy, respectively, and  $T$  is the absolute temperature.

The free energy density for liquid crystalline ordering is expressed in terms of Maier–Saupe (MS) theory for nematic ordering and Chandrasekhar–Clark (CC) theory for hexagonal columnar ordering, viz.<sup>16–18</sup>

$$f^{\text{aniso}} = -\{\Sigma_1 \phi_1 + \Sigma_2 \phi_2\} - \frac{1}{2}\{\nu_{11} \phi_1^2 (s_1^2 + \alpha_1 \eta_1^2) + \nu_{22} s_2^2 \phi_2^2 + 2\nu_{12} \phi_1 \phi_2 (s_1 s_2 + \alpha_{12} \eta_1 \eta_2)\} \quad (2)$$

where  $s_1$  and  $s_2$  are the nematic order parameters, and  $\eta_1$  and  $\eta_2$  are hexagonal columnar order parameters.  $\nu_{11}$  represents the anisotropic interaction within the pure components 1, and  $\nu_{22}$  is that of 2, viz.,  $\nu_j = 4.541 T_{N-I,j}/T$ , where  $T_{N-I,j}$  is the nematic–isotropic transition temperature of component  $j = 1$  or 2.  $\nu_{12}$  is the cross-anisotropic interaction between the two constituents and expressed as:

$$\nu_{12} = c \sqrt{\nu_{11} \nu_{22}} \quad (3)$$

in which  $c$  is the proportionality constant characterizing the relative strength of the cross-interaction between two different mesogens as compared to that in the same species.  $\alpha_1$  and  $\alpha_{12}$  are the coefficients of the hexagonal ordering interaction within the component 1 and the cross-hexagonal ordering interaction between components 1 and 2, respectively.  $\Sigma_1$  and  $\Sigma_2$  are the entropic contribution due to the alignment of individual LC molecules of components 1 and 2, respectively. The entropy term is described as

$$\Sigma_j = \ln Z_j - m_{n,j} s_j - m_{H,j} \eta_j \quad (4)$$

where  $m_{n,j}$  and  $m_{H,j}$  are dimensionless nematic and hexagonal columnar mean field parameters, respectively. The partition function  $Z_j$  and molecular orientation distribution function  $f_j$  are respectively defined as:

$$Z_j = \iiint f_j(\cos \theta, x, y) d \cos \theta dx dy \quad (5)$$

and

$$f_j(x, y, \cos \theta_j) = \exp \left( \frac{1}{2}(3 \cos^2 \theta_j - 1)(m_{n,j} + m_{H,j}[\cos(\tilde{A} \cdot \tilde{r}) + \cos(\tilde{B} \cdot \tilde{r}) + \cos(\tilde{C} \cdot \tilde{r})]) \right) \quad (6)$$

in which  $\tilde{A}$ ,  $\tilde{B}$ , and  $\tilde{C}$  are the primitive vectors of the two-dimensional hexagonal reciprocal lattice, which is given as

$$\tilde{A} = \frac{4\pi}{\sqrt{3}d} \hat{j} \quad (7)$$

$$\tilde{B} = \frac{4\pi}{\sqrt{3}d} \left( \frac{\sqrt{3}}{2} \hat{i} - \frac{1}{2} \hat{j} \right) \quad (8)$$

$$\tilde{C} = \tilde{A} + \tilde{B} = \frac{4\pi}{\sqrt{3}d} \left( \frac{\sqrt{3}}{2} \hat{i} + \frac{1}{2} \hat{j} \right) \quad (9)$$

where  $d$  is the lattice constant. The  $x$ – $y$  integration of the molecular distribution function is carried out over a primitive cell of the two-dimensional hexagonal lattice, and the integration over  $\cos \theta$  is performed from 0 to 1. The nematic and hexagonal columnar order parameters are given respectively as:

$$s_j = \frac{\iiint \frac{1}{2}(3 \cos^2 \theta - 1)f_j(\cos \theta, x, y) d \cos \theta dx dy}{Z_j} \quad (10)$$

and

$$\eta_j = \frac{\iiint \left( \frac{1}{2}(3 \cos^2 \theta - 1)(\cos(\tilde{A} \cdot \tilde{r}) + \cos(\tilde{B} \cdot \tilde{r}) + \cos(\tilde{C} \cdot \tilde{r}))f_j(\cos \theta, x, y) \right) d \cos \theta dx dy}{3Z_j} \quad (11)$$

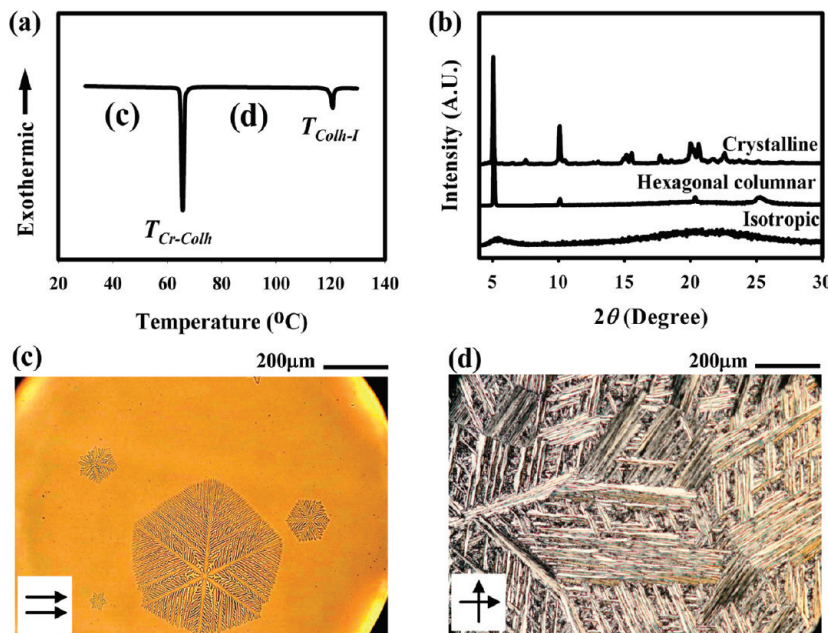


**Figure 1.** (a) DSC thermogram of neat HPTP obtained at a heating rate of 2 °C/min, showing hexagonal columnar–isotropic ( $T_{\text{Colh-I}}$ ) at 121 °C and crystal–columnar ( $T_{\text{Cr-Colh}}$ ) phase transitions at 66 °C. (b) 1D-WAXD scans of HPTP acquired at 25, 68, and 130 °C, corresponding to crystalline, hexagonal columnar liquid crystal, and isotropic states, respectively. Optical micrographs depicting (c) hexagonal columnar liquid crystals at 115 °C and (d) crystalline textures at 25 °C.

By combining Flory–Huggins free energy density of mixing and the anisotropic free energy density, the total free energy density of the binary liquid crystal mixtures covering the hexagonal columnar–nematic–isotropic transition becomes

$$\begin{aligned} f^{\text{total}} &= f^{\text{mixing}} + f^{\text{aniso}} \\ &= \left\{ \frac{\phi_1}{r_1} \ln \phi_1 + \frac{\phi_2}{r_2} \ln \phi_2 + \chi \phi_1 \phi_2 \right\} - \\ &\quad \{ \phi_1 (\ln Z_1 - m_{\text{n},1} s_1 - m_{\text{H},1} \eta_1) + \phi_2 (\ln Z_2 - m_{\text{n},2} s_2 - m_{\text{H},2} \eta_2) \} - \\ &\quad \frac{1}{2} \{ \nu_{11} \phi_1^2 (s_1^2 + \alpha \eta_1^2) + \nu_{22} \phi_2^2 (s_2^2 + \alpha_{12} \eta_1 \eta_2) \} \end{aligned} \quad (12)$$

where the second term in the medium bracket is the entropic contribution to the anisotropic free energy and the third term represents the anisotropic coupling interactions among nematics and columnar LC mesophases. To determine the mesophase transition temperatures, the total free energy of the mixture is first minimized with respect to the individual order parameters ( $s_i$  and  $\eta_i$ ), which yields the following relationships:

$$m_{\text{n},1} = \nu_{11} s_1 \phi_1 + \nu_{12} s_2 \phi_2 \quad (13)$$

$$m_{\text{n},2} = \nu_{22} s_2 \phi_2 + \nu_{12} s_1 \phi_1 \quad (14)$$

$$m_{\text{H},1} = \nu_{11} \alpha_1 \eta_1 \phi_1 + \nu_{12} \alpha_{12} \eta_2 \phi_2 \quad (15)$$

$$m_{\text{H},2} = \nu_{12} \alpha_{12} \eta_1 \phi_1 \quad (16)$$

The order parameters at a given temperature and composition are determined by solving eqs 5, 10, 11, and 13–16. Subsequently, the variation of the total free energy with temperature are computed to determine the phase transition points. Subsequently, the equilibrium coexistence points of the phase

diagrams are further solved by balancing the pseudochemical potential at each phase in the following:

$$\frac{\partial f^{\text{total}}}{\partial \phi_i^\alpha} = \frac{\partial f^{\text{total}}}{\partial \phi_i^\beta} \quad (17)$$

In the determination of the coexistence curves, a common tangent algorithm was employed. The detailed procedure for the construction of the mesophase diagram can be found elsewhere.<sup>19</sup>

## Results and Discussion

Figure 1a exhibits the DSC endotherms of neat HPTP, showing hexagonal columnar–isotropic transition ( $T_{\text{Colh-I}}$ ) at 121 °C and crystal–columnar ( $T_{\text{Cr-Colh}}$ ) transition at 66 °C in a descending order of temperature. To identify these phase transition regions, wide-angle X-ray diffraction (WAXD) experiments were conducted in the  $2\theta$  range of 3 to 30°. In Figure 1b are shown the 1D WAXD scans of neat unaligned HPTP at different temperatures corresponding to the crystalline, columnar LC, and isotropic regions. At 25 °C, the crystalline HPTP shows several distinct diffraction peaks at  $2\theta = 5.1^\circ$ ,  $7.5^\circ$ , and  $10.1^\circ$  (see the upper WAXD scan). In addition, several minor diffraction peaks corresponding to the alkyl chain crystals of HPTP appear in the  $2\theta$  range between  $15^\circ$  and  $23^\circ$ . As the temperature is raised to 68 °C, the diffraction peaks of the crystalline alkyl chains (i.e., between  $15^\circ$  and  $23^\circ$ ) are no longer discernible because of the melting of the aliphatic chain crystals. In the middle WAXD scan of Figure 1b, the HPTP transforms to the hexagonal columnar mesophase as demonstrated by the signature diffraction peaks, representing the hexagonal packing, at  $2\theta = 5.1^\circ$  (corresponding to  $d_{\text{space}}$  of (100) plane is 17.3 Å) and a higher order peak at  $10.1^\circ$ , which gives an intercolumnar distance of 19.9 Å. Meanwhile, the diffraction peaks at  $2\theta = 20.6^\circ$  ( $d_{\text{space}} = 4.3$  Å) and  $25.0^\circ$  ( $d_{\text{space}} = 3.5$  Å) within the columnar mesophase of neat HPTP appear. According to

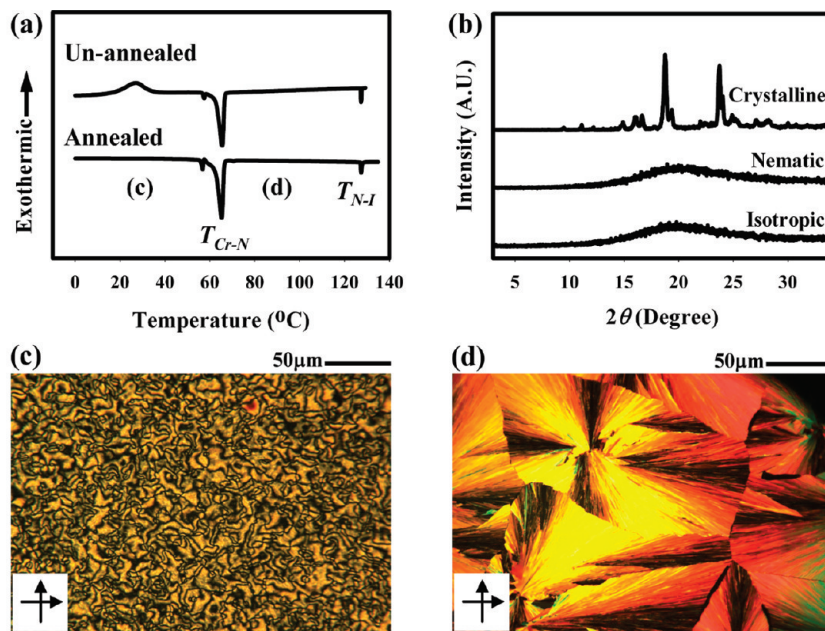


**Figure 2.** (a) DSC thermogram of unannealed and annealed RM257 obtained at a heating rate of 2 °C/min, both showing three endotherms corresponding to the nematic–isotropic ( $T_{N-I}$ ) transition at 127 °C, crystal–nematic ( $T_{Cr-N}$ ) transition at 65 °C, and the melting of metastable crystal at 57 °C. An exotherm at 27 °C is due to the cold crystallization of unannealed RM257. (b) 1D WAXD profiles of RM257 showing the crystalline peaks at 25 °C (top), the broad nematic peak at 68 °C (middle), and the broad amorphous peak in the isotropic state at 130 °C (bottom). The optical micrographs showing (c) the nematic disclinations at 90 °C and (d) the crystalline texture at 25 °C.

Levelut, the former peak can be attributed to the intermolecular distance of the alkyl units and the latter corresponds to the  $\pi-\pi$  stacking distance within the column of liquid crystalline HPTP.<sup>20</sup> In the isotropic state at 130 °C, two very broad diffuse maxima occur at  $2\theta = 5.5^\circ$  ( $d_{space} = 16.0 \text{ \AA}$ ) and  $20.9^\circ$  ( $d_{space} = 4.2 \text{ \AA}$ ), characteristics of average-size HPTP molecules and an average center-of-mass to center-of-mass distance between the neighboring HPTP molecules (see the lower WAXD scan).

To further confirm these crystalline and columnar LC phases, optical micrographs were obtained at the corresponding regions of 115 and 25 °C during the course of cooling from the isotropic melt. As shown in Figure 1c, a six-fold symmetric crystal pattern develops at 115 °C, which is a typical characteristic of a hexagonal columnar phase.<sup>21</sup> With continued cooling to 25 °C, the dendrite-like crystalline morphology of HPTP appears (Figure 1d). These optical micrographs are in good accord with those observed for crystalline and columnar phases in the DSC and WAXD experiments.

Similar experiments were carried out for neat RM257. Figure 2a shows the DSC scans of the unannealed and annealed (for 24 h at 40 °C) samples. In the former, three endotherms appear at 57, 65, and 127 °C and one exotherm appears at 27 °C during the heating cycle. The exotherm is attributed to cold crystallization of RM257. The highest peak corresponds to the nematic–isotropic ( $T_{N-I}$ ) phase transitions (i.e., 127 °C), whereas the primary peak at 65 °C is ascribed to the crystal–nematic ( $T_{Cr-N}$ ) transition (Figure 2a). The DSC thermograms of the annealed RM257 are comparable to those of the unannealed sample, except that the area under the crystal melting peak is slightly larger, suggesting enhanced crystallinity upon annealing. The cold crystallization peak of RM257 during the heating cycle was no longer observable in the annealed specimens because of the nonthermal equilibrium nature of the slowly crystallizing RM257. The minor endotherm at around 57 °C is ascribed to the melting of the unstable crystals arising from the cold crystallization, but the unambiguous assignment of this minor endothermic peak is not possible because it still

persists in the annealed sample. Nevertheless, it does not affect the assignment of the melting point of the RM257 crystal. The minuteness of this minor peak implies that the annealing process cannot eliminate the cold crystallization completely. Because this small endothermic peak is no longer observable in its blends with HPTP, we shall only focus on the trends of the primary melting peak of RM257.

In the X-ray diffraction scan of the RM257 crystal at 25 °C, several diffraction peaks are evident (the upper WAXD scan, Figure 2b), but only two peaks located at  $2\theta = 18.7^\circ$  ( $d_{space} = 4.7 \text{ \AA}$ ) and  $23.7^\circ$  ( $d_{space} = 3.7 \text{ \AA}$ ) are pronounced. Because of the limited numbers of diffraction peaks available, we do not attempt to determine the unit cell structure of the RM257 crystal. The 1D WAXD scans of nematic and isotropic states of RM257 were acquired at 68 and 130 °C, respectively. A broad nematic diffuse peak is observed at  $2\theta = 19^\circ$  as seen in the middle WAXD scan of Figure 2b. This broad nematic scattering is comparable to that of the amorphous scattering in the isotropic state, suggesting that the center-of-mass to center-of-mass distance between RM257 molecules in the nematic state and in the isotropic melt are practically comparable. This observation is not surprising because there is no positional ordering in the nematic state; the WAXD scans in the nematic and isotropic states would thus be indistinguishable in the  $2\theta$  scans. As depicted in Figure 2c,d, the polarized optical micrographs of RM257 taken at 90 and 25 °C show the nematic disclinations, and the large spherulitic structures with Maltese-crossed patterns confirm the corresponding nematic and crystalline regions obtained by the DSC and WAXD investigations. From the distinctive differences between mesophase regions in the WAXD scans of HPTP and RM257, the emerged mesophase structures and the relevant coexistence regions of the phase diagram of the present HPTP/RM257 mixtures can be assigned.

Figure 3 shows the DSC thermograms of the HPTP/RM257 mixtures covering the (a) low (50–80 °C) and (b) high (75–130 °C) temperature regions over the entire range of compositions at 10 wt % increments. The endothermic peak of the neat HPTP

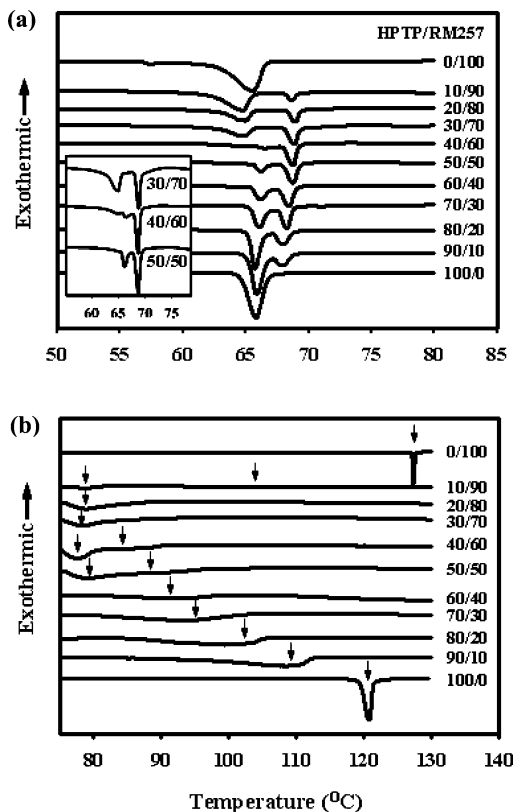


**Figure 3.** (a) DSC thermograms of HPTP/RM257 mixtures, exhibiting various phase transitions obtained at a heating rate of 2 °C/min and showing little or no change in the melting points of neat HPTP (66 °C) and RM257 (65 °C), with the development of new endothermic peaks at 68 °C in the mixtures that are absent in the neat components. The inset displays the enlarged DSC thermogram of the 30/70, 40/60, and 50/50 compositions showing the two melting peaks corresponding to HPTP and RM257 and an additional endothermic peak in the 40/60 composition. (b) Phase transition of the mesophase (arrow), showing a eutectic phase behavior with a minimum at 78 °C in the vicinity of the 30/70 composition.

crystal is located at 66 °C, while the crystal melting peak of neat RM257 appears around 65 °C. As shown in Figure 3a, upon blending, most compositions exhibit two melting endotherms; the lower temperature peaks correspond to either of the neat constituents. In the case of the 40/60 HPTP/RM257 composition, three endothermic peaks are clearly discerned as shown in the inset; the two peaks at the lower temperatures are the melting transitions of the neat crystalline constituents. The melting peak of the HPTP crystal remains virtually stationary upon blending, whereas the RM257 crystal shows slight depression of the melting temperatures. The appearance of a higher temperature endothermic peak is unusual, which occurs a few degrees higher (i.e., at about 68 °C) than that of the constituent crystals and is absent in the neat constituents (Figure 3a). This higher temperature peak is regarded as an induced ordered phase, which is thermally more stable relative to those of the constituent crystals.

When the temperature is raised above 70 °C (i.e., the mesophase transition temperature of the induced phase), the HPTP crystal melts to a hexagonal columnar phase, while the RM257 crystal transforms to a nematic phase. As indicated by the arrows in Figure 3b, a systematic depression of the mesophase–isotropic phase transition temperature occurs in both the hexagonal columnar HPTP and nematics of RM257, showing a eutectic point in the composition range between 20/80 and 30/70 at approximately 78–80 °C.

Evidently, the DSC thermograms of HPTP/RM257 alone may be inadequate to elucidate the phase behavior of the mixtures; thus, a POM study was conducted to mimic the morphology development associated with these mesophase transitions during the course of cooling and heating cycles. Figure 4 exhibits the emerged morphology of the 80/20 HPTP/RM257 composition during cooling. At 97 °C, very faint six-fold crystal textures, characteristic of the hexagonal columnar liquid crystalline phase, emerge from the isotropic melt under parallel polarization (Figure 4a). Upon cooling to 76 °C, the columnar domains grow and eventually impinge into each other. This impinged texture is clearly seen under the cross-polarization (Figure 4b) at the same temperature, suggesting that the LC directors probably deviate from the ideal homeotropic alignment because of the impingement effect. As depicted in the micrograph of Figure 4c at 40 °C, the hexagonal columnar phase of HPTP gradually transforms to the solid crystals; this crystal solidification is seemingly completed at 38 °C (Figure 4d).

In the case of the 20/80 HPTP/RM257 mixture, multiple tiny droplets develop, suggestive of liquid–liquid phase separation at 85 °C (Figure 5a). Concurrently, some droplets show bright birefringent appearance, indicating the formation of nematic disclinations within the phase-separated domains in the continuum of isotropic fluid (Figure 5a). This observation implies that the nematic ordering lags behind the liquid–liquid phase separation. The dispersed nematic domains in the matrix of isotropic liquid are the signature of the nematic + isotropic coexistence phase. These nematic domains grow through coalescence with continued cooling (Figure 5b) and form an oily streak texture at 70 °C (Figure 5c). The oily streaks and polydomains both reveal disclination textures, implying a characteristic of liquid crystalline ordering. As the temperature is further reduced to 40 °C, the oily streak domains transform to the crystals that grow toward the dark regions (Figure 5d). Upon cooling to 30 °C and annealing isothermally for 95 min, the crystallization predominates over the polydomains (Figure 5e,f). This observation is attributed to the slow crystallization of RM257. The optical results suggest that the oily streaks are associated with the HPTP-rich region and that the polydomains are attributable to the RM257-rich region. Although the development of intricate mesophase structure during cooling is interesting, it is extremely difficult to unambiguously determine the phase transition temperatures from the cooling runs because of the nonequilibrium nature of the crystal growth dynamics of the mesophases caused by the changing supercooling during the cooling. Hence, we shall focus on the POM heating runs.

Figure 6 shows the morphology evolution in the 40/60 HPTP/RM257 composition during the course of heating under cross-polarization. At 30 °C, a spherulitic structure develops as demonstrated by the large Maltese-cross pattern under cross-polarization (Figure 6a). In the enlarged view, a sizable number of small crystals with irregular six-fold patterns are dispersed within the spherulite, indicating the coexistence of two types of crystals (Figure 6b). As the temperature is raised to 66 °C, the spherulite melts to a mesophase (i.e., nematics of the RM257-rich phase), but no obvious change in the shape occurs in the dispersed crystals, except that the color contrast gets weaker (Figure 6c). However, this phase transition behavior is more pronounced in the DSC experiment (Figure 3a, inset). Upon heating to 70 °C, the texture in the matrix remains unchanged, but the intricate texture within the dispersed crystals melts while maintaining the six-fold irregular pattern without any internal texture, suggestive of a hexagonal columnar LC. The dark appearance under cross-polarization suggests that some

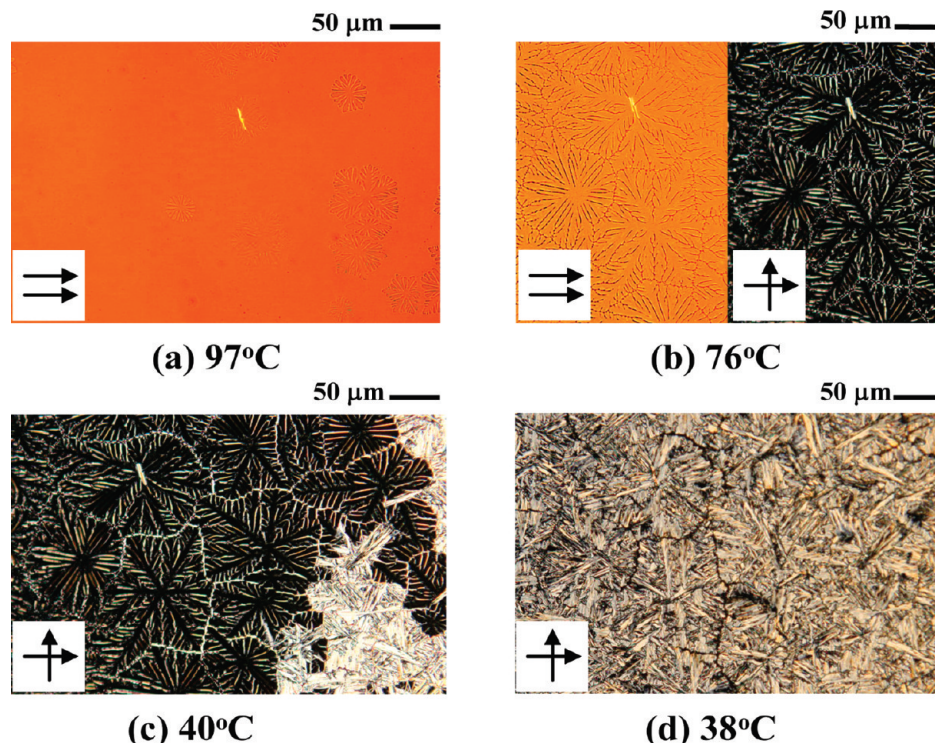


**Figure 4.** Optical micrographs of the 80/20 HPTP/RM257 composition acquired during the course of cooling, showing (a) the isotropic–columnar transition at 97 °C, (b) the impingement of columnar phase at 76 °C, (c) emerged crystalline texture at 40 °C, and (d) crystalline texture at 38 °C.

of these columnar LC molecules are homeotropically aligned, except for those near or at the interface (Figure 6d). When the temperature reaches 78 °C, the continuous mesophase completely transforms to the isotropic melt, whereas the irregular six-fold domains still persist (Figure 6e). With further increase of temperature, the irregular six-fold domains gradually melt (Figure 6f) and become completely isotropic at 96 °C with dark appearance (picture not shown).

On the basis of the DSC and POM observations, the phase transition temperatures of the HPTP/RM257 blends were plotted against the weight fraction of HPTP in Figure 7. As pointed out previously, the nematic–isotropic transition of RM257 appears at 127 °C whereas the hexagonal columnar–isotropic transition occurs at 121 °C. Upon blending, both transitions show depressed trends with the minimum in the vicinity of 78–80 °C at the 30/70 composition of HPTP/RM257, suggesting eutectic melting. At lower temperatures, the melting transitions of both constituents are found to be so close (i.e., 65 and 66 °C) as to virtually overlap in their blends. However, a systematic trend appears in the enlarged plot of the inset. The melting temperature of both components remains unchanged in the mixtures, except that there is a more stable phase at a temperature above the melting temperature of the constituent crystals, which is reminiscent of an upper azeotrope. The origin of this stable phase will be discussed in the subsequent section based on the WAXD experiment.

Figure 8a exhibits the 1D WAXD scans of the 100/0, 80/20, 20/80, and 0/100 HPTP/RM257 compositions acquired at 25 °C. The assignments of the individual peaks of the neat constituents are described in Figures 1 and 2. In the diffraction profile of the 80/20 composition, the diffraction peaks in  $2\theta = 18.7^\circ$  and  $19.4^\circ$  corresponding to crystalline RM257 are no longer observable, whereas the signature peak of alkyl chain crystals of HPTP located between  $15^\circ$  and  $16^\circ$  and between  $20^\circ$  and  $21^\circ$  still persist. In the enlarged scans as shown in Figure

8b, an induced peak, which is absent in the pure components, is evident at  $2\theta = 19.7^\circ$  in the mixture as indicated by the arrows, suggesting the formation of the induced phase. In the case of the 20/80 composition, the induced peak and the peaks of crystalline RM257 are still discernible in its corresponding profile, but the characteristic peaks of alkyl chain crystals of HPTP disappear. However, the other diffraction peaks corresponding to HPTP core molecules still remain. According to the above observation and DSC result, the appearance of the induced peak suggests the formation of a new phase in the mixture of HPTP and RM257, and the wide-angle X-ray diffraction profiles of the 80/20 and 20/80 compositions indicate the coexistence of the induced ordered phase + crystalline HPTP and the induced ordered phase + crystalline RM257 in the respective regions.

To further confirm the induced phase, the WAXD experiments were performed at different temperatures. Figure 9 shows the  $2\theta$  scans of the 80/20 and 20/80 HPTP/RM257 compositions and the neat components at (a) 66 °C and (b) 70 °C. At 66 °C, HPTP and RM257 show the WAXD profiles of the neat mesophases as depicted in Figure 1 and 2; however, the mixtures show considerably different profiles from the liquid crystalline phases of the neat constituents (Figure 9a). This result further confirms the formation of the induced phase in the mixed state of HPTP and RM257. Besides, the  $2\theta$  ratio between the first three peaks, i.e.,  $2\theta = 5.0^\circ : 2\theta = 9.9^\circ : 2\theta = 14.8^\circ \cong 1:2:3$ , implies that the induced phase is highly ordered relative to the  $\text{Col}_h$  phase. According to the POM result (Figure 6c), the dispersed entities show a crystal-like texture, drastically different from that of the  $\text{Col}_h$  phase. Hence, it is reasonable to assign this induced ordered phase to the induced crystalline phase ( $\text{Cr}_{in}$ ). As shown in the inset, the enlarged WAXD scans (at low  $2\theta$ ) of the 80/20 HPTP/RM257 composition shows dual peaks at  $2\theta = 4.9^\circ$  and  $2\theta = 5.1^\circ$ , indicating the coexistence of  $\text{Col}_h + \text{Cr}_{in}$ . In contrast, the WAXD scan of the 20/80 composition

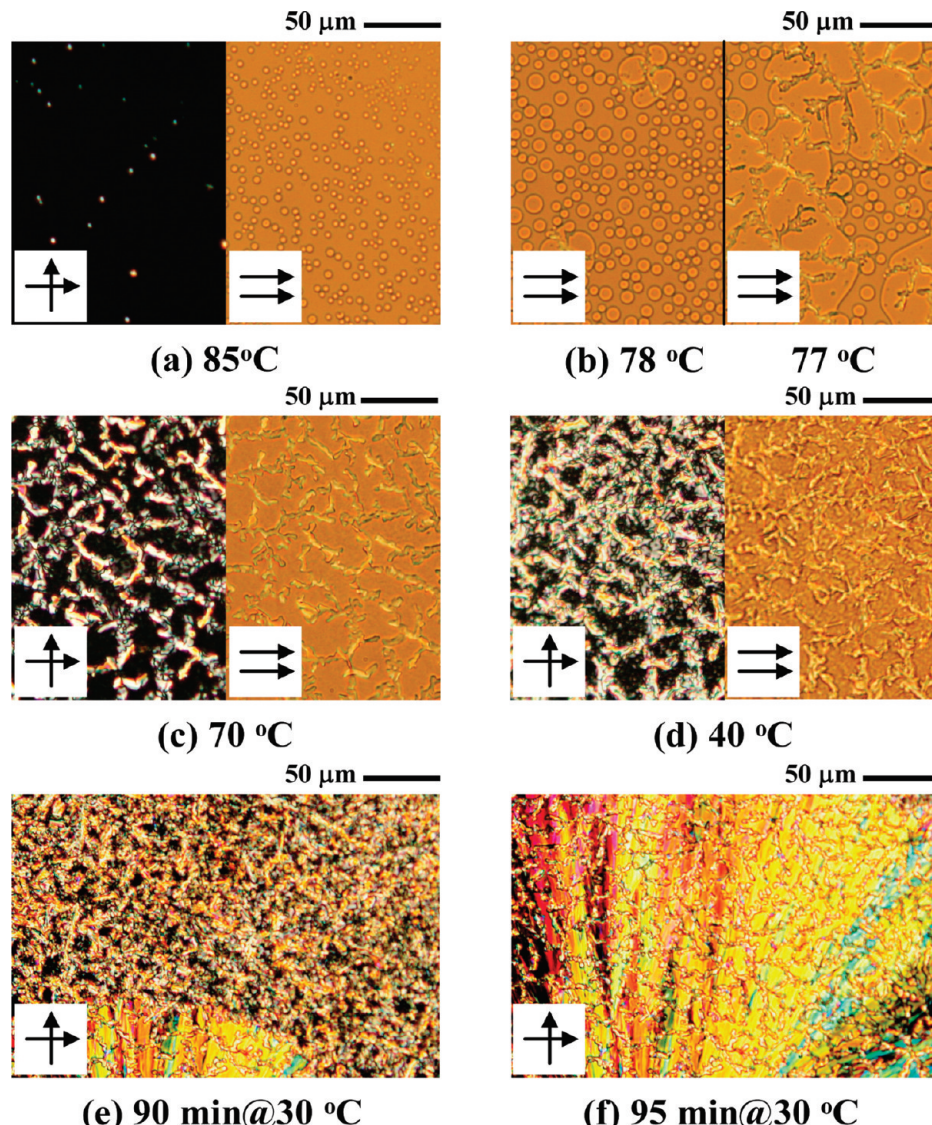


**Figure 5.** Optical micrographs of the 20/80 HPTP/RM257 composition during the course of cooling, showing (a) isotropic–nematic transition at 85 °C. (b) The coalescence of droplets with decreasing temperature, forming (c) oil streak structure. (d) The crystallization of oily streaks at 40 °C. (e) The onset of crystallization of the second component. (f) Predominant crystal growth over the existing polydomains at 30 °C with annealing time.

shows only a single peak at  $2\theta = 4.9^\circ$ , suggestive of the coexistence of  $\text{Cr}_{\text{in}} + \text{N}$ , because there is no pronounced diffraction peak in the nematic state.

As the temperature is raised to 70 °C, where the induced crystalline phase melts, all the mixtures show a sharp peak at  $2\theta = 5.1^\circ$  and a broad peak at  $2\theta = 25.3^\circ$  (Figure 9b). In the 80/20 composition, the highly ordered diffraction peak of  $\text{Col}_h$  becomes weaker, but it is still discernible at  $2\theta = 10.1^\circ$ . With increasing RM257 content, this diffraction peak eventually disappears. However, the development of  $\text{Col}_h$  phase in the mixtures is clearly identified by the six-fold crystal texture during cooling under optical microscopic investigation. Therefore, the absence of the higher order peaks seems to suggest the lesser correlation of the  $\text{Col}_h$  phase with the addition of RM257. Besides, the diffuse scattering attributable to the nematic phase becomes more prominent with increasing RM257 concentration (Figure 9b). More importantly, the above WAXD scan of the mixtures at 70 °C confirms the coexistence of  $\text{Col}_h + \text{N}$ .

On the basis of the above WAXD and DSC investigations, the low temperature part (i.e., 60–70 °C) of the phase diagram

of HPTP/RM257 mixtures is constructed as depicted in Figure 10. Below the melting temperature of pure constituents, the induced crystalline phase that only exists in the mixed HPTP/RM257 emerges, which is surrounded by the two coexistence regions,  $\text{Cr}_2$  (RM257) +  $\text{Cr}_{\text{in}}$  in the RM257-rich and  $\text{Cr}_{\text{in}} + \text{Cr}_1$  (HPTP) in the HPTP-rich compositions. With increasing temperature, the HPTP and RM257 crystals in the mixtures transform to their corresponding mesophase, showing the  $\text{N} + \text{Cr}_{\text{in}}$  and  $\text{Cr}_{\text{in}} + \text{Col}_h$  coexistence regions. Above the transition temperature of the induced crystal, i.e., 68 °C, the  $\text{Col}_h + \text{N}$  coexistence region is discerned.

The higher temperature portion of the experimental phase diagram of HPTP/RM257 blends may be further compared with the theoretical phase diagram, calculated self-consistently in the framework of the combined free energies of Flory–Huggins free energy of liquid–liquid phase separation, Maier–Saupe free energy of nematic ordering, and Chandrasekhar–Clark free energy of hexagonal columnar packing. In the calculation, the hexagonal ordering interaction and cross-hexagonal ordering interaction parameters were set to  $\alpha_1 = 1.01$  and  $\alpha_{12} = 0.01$ ,

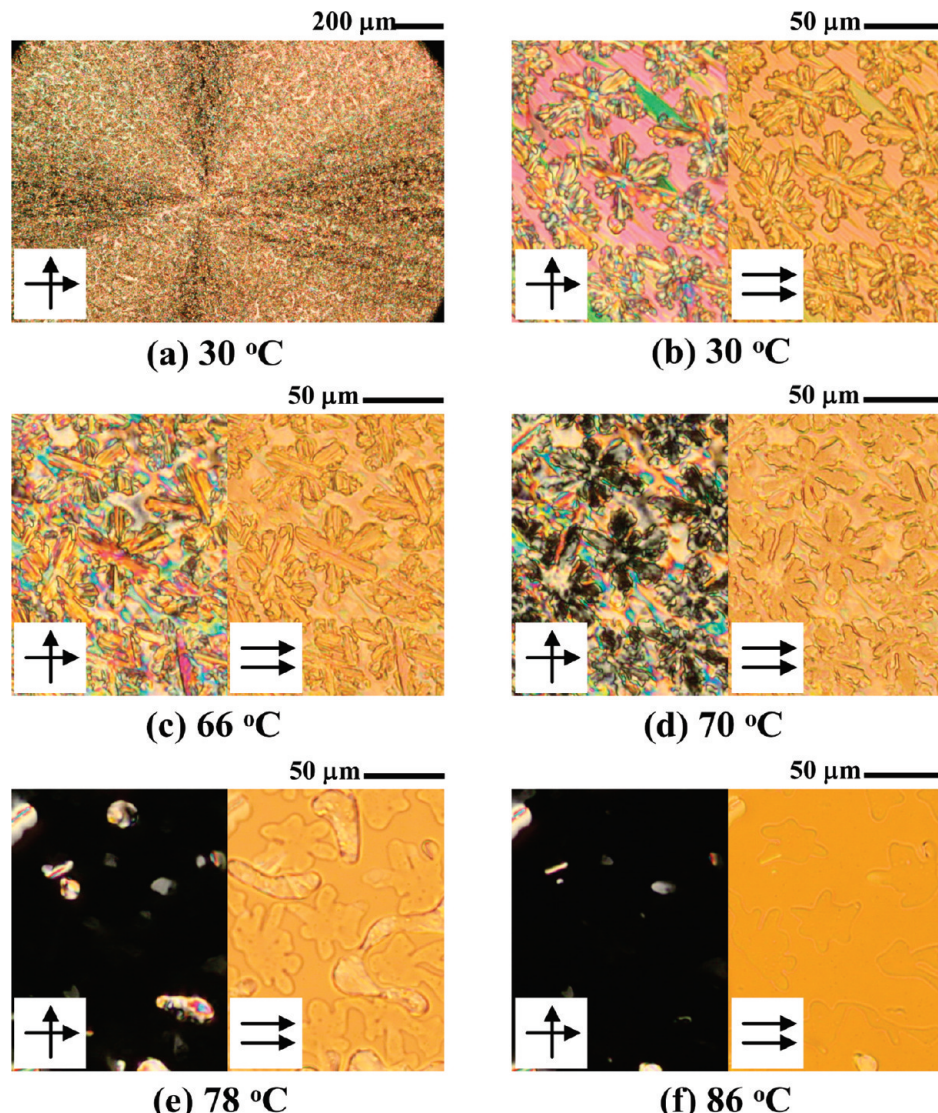


**Figure 6.** (a) Optical micrographs of the 40/60 HPTP/RM257 composition during heating, showing a spherulitic structure with a Maltese-cross pattern at 30 °C. (b–f) Magnified (8×) images of part a, showing (b) numerous crystals with six-fold symmetry of HPTP dispersed within the preformed spherulitic matrix crystal, (c) melting of the spherulite matrix to nematics at 66 °C, (d) the melting of six-fold crystals at 70 °C, (e) the nematic–isotropic transition of the matrix at 78 °C, and (f) the melting of the Col<sub>h</sub> to isotropic phase at 86 °C.

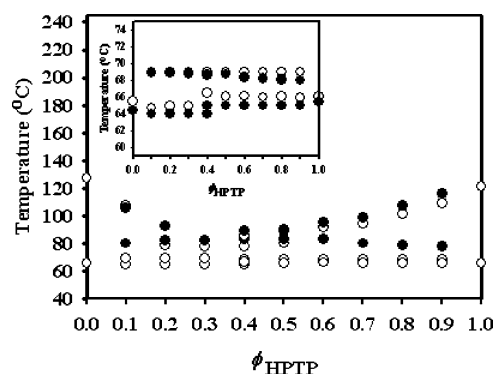


**Figure 7.** Plots of phase transition temperatures versus HPTP composition of the HPTP/RM257 blends. The phase transition points as determined by DSC and optical microscopy are indicated by open ( $\circ$ ) and filled ( $\bullet$ ) symbols, respectively, showing a eutectic behavior of mesophase–isotropic transitions and the melting points in a descending order of temperature. The phase transition at 80 °C refers to the eutectic line. Below the eutectic line, a broad Col<sub>h</sub> + N coexistence region is discernible. A single nematic phase gap is clearly discernible in some RM257-rich compositions, but the Col<sub>h</sub> gap is extremely narrow as though it coincided with the neat HPTP liquid crystal.

respectively, along with the cross-anisotropic interaction parameter  $c = 0.77$ . Other parameters used were  $T_{\text{crit}} = -48$  °C,

$$A = -3.7, r_1 = 3 \text{ for HPTP (implying three phenylene arms), and } r_2 = 1 \text{ for RM257.}$$

The present theory covers only the nematic–isotropic transition of RM257 and hexagonal columnar–isotropic transition of HPTP; the low temperature crystalline phase and the induced crystalline phase were temporally ignored here. The detailed theoretical deduction and computation on the complete eutectic mesophase including the induced crystalline phase will be presented in a future paper. In the phase diagram, the mesophase–isotropic phase (i.e., Col<sub>h</sub>–I and N–I) transition temperatures are depressed by addition of the other constituent, showing a eutectic point in the vicinity of the 25/75 HPTP/RM257 composition around 80 °C. The coexistence of nematic + isotropic (N + I) and hexagonal columnar + isotropic (Col<sub>h</sub> + I) bound by the solidus and liquidus lines are presented. The phase transition at 80 °C refers to the eutectic line. Below the eutectic line, a broad Col<sub>h</sub> + N coexistence region is discernible. A single nematic phase gap is clearly discernible in some RM257-rich compositions, but the Col<sub>h</sub> gap is extremely narrow as though it coincided with the neat HPTP liquid crystal.

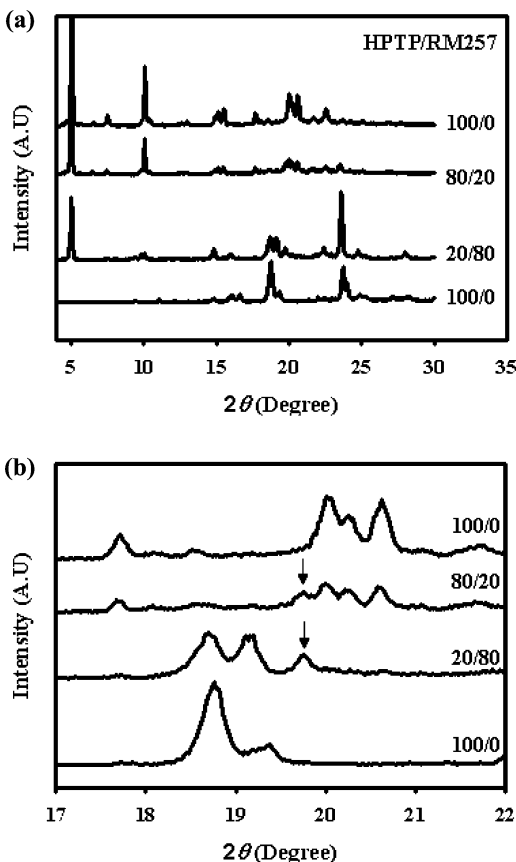


**Figure 8.** (a) Comparison of 1D WAXD scans of 100/0, 80/20, 20/80, and 0/100 HPTP/RM257 mixtures acquired at room temperature. (b) The enlarged diffraction profiles in the  $2\theta$  range between 17° and 21° that show evidence of a new peak at  $2\theta = 19.7^\circ$  (indicated by arrows) in the 80/20 and 20/80 mixtures, indicating the induced ordered phase in the mixed HPTP/RM257 crystals.

The coexistence regions obtained by the theoretical calculation can be confirmed by thermal quenching at various compositions from the isotropic melt to different temperatures corresponding to various coexistence regions. Figure 11a displays the morphology in the blend of 10/90 HPTP/RM257 following a thermal quench from the isotropic melt to 98 °C. Anisotropic droplets with distinct Schlieren texture, i.e., a typical characteristic of nematic LC, initially emerge and then grow to larger domains with elapsed time. More importantly, these droplets are surrounded by the isotropic melt, suggestive of the nematic + isotropic (N + I) coexistence region. In the case of a deeper thermal quench from the isotropic melt to 95 °C, the 10/90 mixture shows disclination textures, suggestive of the single nematic LC (Figure 11b). Upon quenching from 130 to 75 °C, the mixture initially shows a single nematic phase, and as time elapses, a secondary phase, i.e., hexagonal columnar phase, starts to emerge from the homogeneous nematic phase (Figure 11c). This result indicates the  $\text{Col}_h + \text{N}$  coexistence region. This coexistence region is also confirmed by a thermal quench experiment from 130 to 75 °C in both 50/50 and 90/10 HPTP/RM257 compositions. In the case of the 50/50 mixture, the development of the nematic Schlieren texture and hexagonal columnar structure is shown in Figure 11d. In the case of the 90/10 blend, the columnar LC shows a mosaic texture, while the nematic disclination (i.e., Schlieren texture) is discerned in the intermediate region between the neighboring hexagonal columnar domains (Figure 11e). On the other hand, Figure 11f exhibits the morphology of the 70/30 composition upon thermal quenching from 130 to 90 °C, showing irregular degenerate

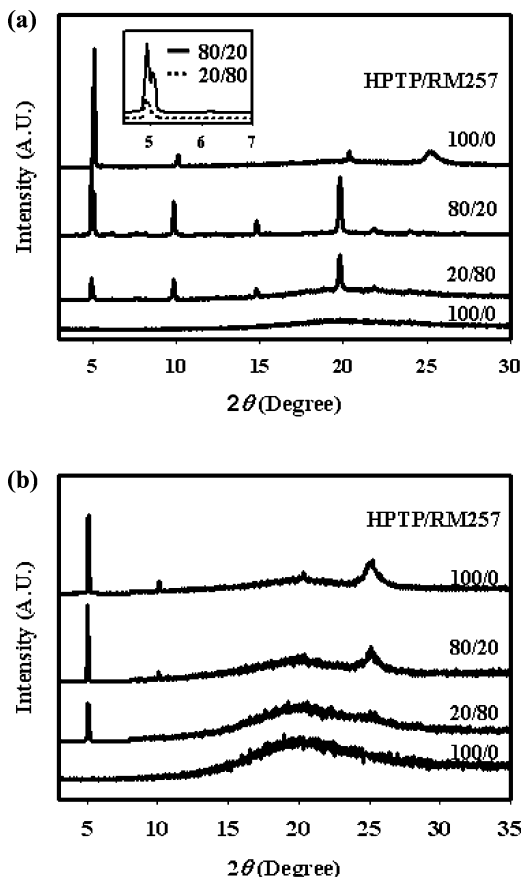


**Figure 9.** Comparison of 1D WAXD profiles among the 100/0, 80/20, 20/80, and 0/100 HPTP/RM257 compositions acquired at (a) 66 °C and (b) 70 °C. (a) At 66 °C, the mixtures show new diffraction peaks in the WAXD scans as compared to the neat constituents, implying the formation of the induced phase in the HPTP/RM257 mixture. The inset shows the dual and single peaks in the enlarged WAXD profiles of the  $\text{Col}_h + \text{Cr}_{in}$  and the  $\text{Cr}_{in} + \text{N}$  coexistence phases in the 80/20 and 20/80 compositions, respectively. (b) At 70 °C, the WAXD profiles of the 80/20 and 20/80 mixtures show a combination of the diffraction peaks corresponding to the HPTP columnar phase and the diffuse maxima (at  $2\theta = 20^\circ$ ) of the RM257, suggesting the  $\text{Col}_h + \text{N}$  coexistence phase.

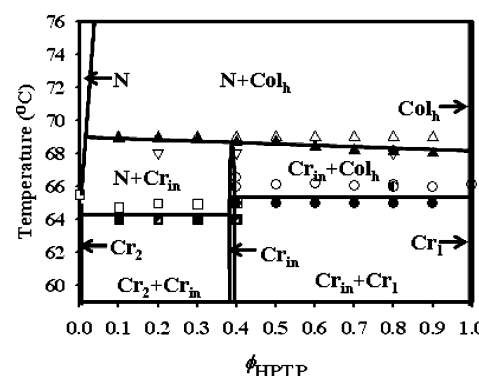


**Figure 10.** Experimental phase diagram of HPTP/RM257 mixtures at a temperature below the melting temperatures of the neat constituents, showing the  $\text{Cr}_{in} + \text{Cr}_1$  and  $\text{Cr}_2 + \text{Cr}_{in}$  coexistence separated by the  $\text{Cr}_{in}$  region. As the temperature is raised, these coexistence regions transform to the  $\text{N} + \text{Cr}_{in}$  and  $\text{Cr}_{in} + \text{Col}_h$  coexistence regions as the individual crystals of the neat constituents melt. When the induced crystal melts to the respective mesophases, the  $\text{Col}_h + \text{N}$  region and a single N gap develop. Triangles:  $\text{Cr}_{in}$ —mesophase transition (open: DSC, filled: POM, and inverted: WAXD). Squares: melting of the RM257 crystal (open: DSC, filled: POM, and semifilled: WAXD). Circles: melting of HPTP crystals (open: DSC, filled: POM, and semifilled: WAXD).

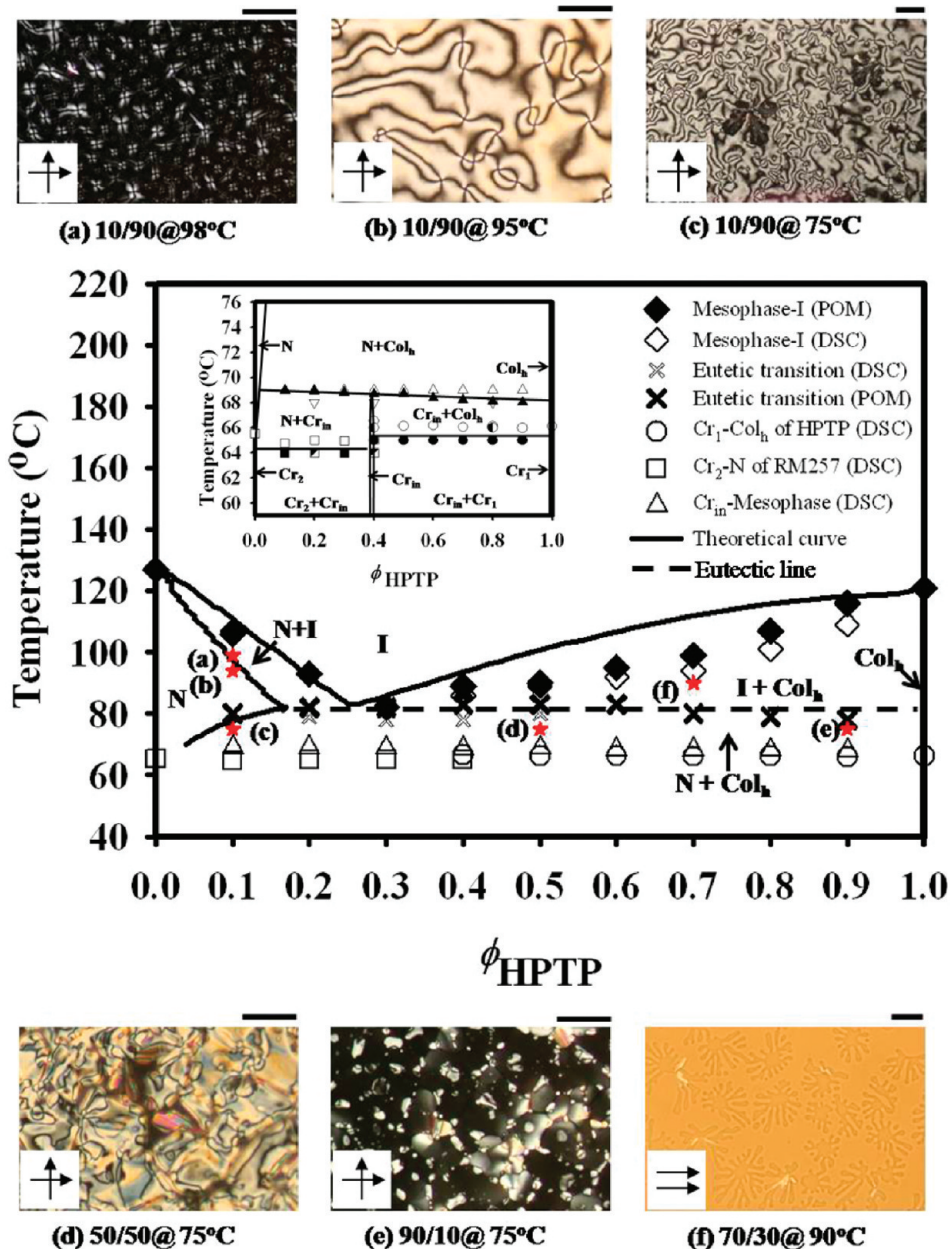


**Figure 11.** Comparison between the self-consistently calculated lines and the experimental phase transition temperatures of HPHP/RM257 blends, showing a eutectic phase behavior of the mixtures. The inset displays the low temperature part of the phase diagram covering the induced crystal gap. The optical micrographs of the thermal-quenched experiments from isotropic region to various coexistence regions above the melting temperatures of the induced crystals: (a) N + I, (b) single N, (c, d, e) Col<sub>h</sub> + N, and (f) Col<sub>h</sub> + I coexistence regions. The scale bar is 50  $\mu$ m.

morphology and indicating imperfect hexagonal columnar LC in the continuum of the isotropic melt, thereby confirming the Col<sub>h</sub> + I coexistence region.

### Conclusions

This study demonstrates, for the first time, that a eutectic phase diagram of the hexagonal columnar liquid crystal system can be described by means of a combination of Flory–Huggins free energy of isotropic mixing, Maier–Saupe free energy of nematic ordering, and Chandrasekhar–Clark free energy of hexagonal columnar ordering. We have demonstrated that the self-consistently calculated phase diagram HPTP/RM257 blend is essentially a eutectic type, consisting of isotropic (I), nematic (N), and hexagonal columnar (Col<sub>h</sub>) regions, and the nematic + isotropic (N + I), hexagonal columnar + isotropic (Col<sub>h</sub> + I), hexagonal columnar + nematic (Col<sub>h</sub> + N) coexistence

regions, bound by the liquidus and solidus lines. Upon lowering the temperature, an induced crystalline phase (Cr<sub>in</sub>) is formed in the intermediate compositions of the HPTP/RM257 mixture, as demonstrated by the observed Cr<sub>2</sub> + Cr<sub>in</sub> and Cr<sub>in</sub> + Cr<sub>1</sub> coexistence phases. When the individual neat crystals melt to the respective columnar and nematic mesophases, the Cr<sub>in</sub> + Col<sub>h</sub> and N + Cr<sub>in</sub> regions can be identified by WAXD. The observed eutectic mesophase behavior and the induced crystalline phase in the intermediate compositions of the HPTP/RM257 mixtures are completely new for the hexagonal columnar liquid crystal systems.

**Acknowledgment.** Support of this work by the National Science Foundation, Division of Materials Research, through Grant number DMR-0514942 is gratefully acknowledged. The

authors are indebted to Dr. S. Z. D. Cheng and his group for their assistance in the WAXD experiments.

## References and Notes

- (1) Popem, M.; Swenberg, C. E. *Electronic Processes in Organic Crystals*; Oxford University Press: New York, 1982.
- (2) Boden, N.; Bushby, R. J.; Clements, J. *J. Mater. Sci. Mater. Electron.* **1994**, *5*, 83–88.
- (3) Adam, D.; Schuhmacher, P.; Simmerer, J.; Haeussling, L.; Siemensmeyer, K.; Etzbach, K. H.; Ringsdorf, H.; Haarer, D. *Nature* **1994**, *371*, 141–143.
- (4) Freudenmann, R.; Behnisch, B.; Hanack, M. *J. Mater. Chem.* **2001**, *11*, 1618–1624.
- (5) van de Craats, A. M.; Stutzmann, N.; Bunk, O.; Nielsen, M. M.; Watson, M.; Mullen, K.; Chanzy, H. D.; Sirringhaus, H.; Friend, R. H. *Adv. Mater.* **2003**, *15*, 495–499.
- (6) O'Neill, M.; Kelly, S. M. *Adv. Mater.* **2003**, *15*, 1135–1146.
- (7) Schmidt-Mende, L.; Fechtenkotter, A.; Mullen, K.; Moons, E.; Friend, R. H.; MacKenzie, J. D. *Science* **2001**, *293*, 1119–1122.
- (8) Fox, M. A.; Grant, J. V.; Melamed, D.; Torimoto, T.; Liu, C.-Y.; Bard, A. J. *Chem. Mater.* **1998**, *10*, 1771–1776.
- (9) Itoh, T.; Takada, A.; Fukuda, T.; Miyamoto, T.; Yakoh, Y.; Watanabe, J. *Liq. Cryst.* **1991**, *15*, 221–228.
- (10) Kang, S.-W.; Li, Q.; Chapman, B. D.; Pindak, R.; Cross, J. O.; Li, L.; Nakata, M.; Kumar, S. *Chem. Mater.* **2007**, *19*, 5657–5663.
- (11) Yandek, G. R.; Meng, S.; Sigalov, G. M.; Kyu, T. *Liq. Cryst.* **2006**, *33*, 775–788.
- (12) Park, S.; Kyu, T. *J. Chem. Phys.* **2008**, *129*, 244901–9.
- (13) Boden, N.; Borner, R. C.; Bushby, R. J.; Cammidge, A. N.; Jesudason, M. V. *Liq. Cryst.* **1993**, *15*, 851–858.
- (14) Flory, P. J. *Principles of Polymer Chemistry*; Cornell University Press: Ithaca, NY, 1953.
- (15) Huggins, M. L. *J. Am. Chem. Soc.* **1942**, *64*, 1712–1719.
- (16) Feldkamp, G. E.; Handchy, M. A.; Clark, N. A. *Phys. Lett. A* **1981**, *85A*, 359–362.
- (17) Chandrasekhar, S.; Savihramma, K. L.; Madusudana, N. V. *ACS Symposium on Ordered Fluids and Liquid Crystals*; Plenum Press: New York, 1982, Vol. 4, p 299.
- (18) Maier, W.; Saupe, A. Z. *Naturforsch.* **1959**, *14*, 882–889, 1960, *15*, 287–292.
- (19) Shen, C.; Kyu, T. *J. Chem. Phys.* **1995**, *102*, 556–562.
- (20) Levelut, A. M. *J. Phys. Lett. (France)* **1979**, *40*, L81–L84.
- (21) Chandrasekhar, S. *Liquid Crystals*; Cambridge University: Cambridge, 1992.

JP1048293